6D Self-Calibration of the Position and Orientation of Radar Sensors in a Radar Network

DOI: 10.23919/EuRAD54643.2022.9924790

6D Self-Calibration of the Position and Orientation of Radar Sensors in a Radar Network

Timo Grebner, Matthias Linder, Nicolai Kern, Pirmin Schoeder, Christian Waldschmidt
Institute of Microwave Engineering, Ulm University, Germany
{name.surname}@uni-ulm.de

***Abstract*— Nowadays, radar sensor networks are often used for modern driver assistance systems in order to generate robust and precise environmental representations. The quality of the environment mapping depends significantly on the accurate knowledge of the mounting position and orientation of the radar sensors. In particular, both the relative orientation and positioning with respect to the other sensors are of great importance. In this paper, an algorithm is presented which performs an estimation of the relative orientation around all three rotation axes as well as the relative position in all three dimensions of distributed radar sensors. For this purpose, only an overlapping field of view (FoV) of the sensors as well as a moving point target, e.g. a corner reflector, which moves along an arbitrary trajectory without the need to know its position and velocity, is required. The estimation accuracy verified with the help of measurements is up to $4\,\mathrm{cm}$ for the position and $0.35°$ for the orientation in 3D space.**

***Keywords*— chirp-sequence radar sensor, multilateration, self-calibration, radar network**

I. Introduction

Modern Advanced Driver Assistance Systems (ADAS) rely on high-precision environmental perception as well as accurate speed and position information, which can be estimated very robustly with radar sensors. Today, radar sensor networks are often used to observe identical targets under different directions of arrival in order to localize them more accurately or to estimate a motion vector instantaneously [1], [2]. In order to ensure high precision, both intrinsic error influences, like array calibration, and extrinsic error influences, such as incorrect relative orientation and position of the sensors in relation to each other, must be minimized. While there are various calibration options for intrinsic errors [3], [4], which have also become increasingly efficient over time [5], methods for the extrinsic calibration of the sensors are often complex or require certain prerequisites. Moreover, they often only allow either orientation estimation or position estimation, but not both at the same time.

The authors in [6] and [7] could already show that on the basis of known sensor positions the orientations of the sensors around the local z-axis can be precisely determined according to the coordinate definition shown in Fig. 1. However, this requires a time-synchronized IMU or GNSS and only the sensor orientation in one dimension can be accurately estimated. A possibility to estimate both the position and the orientation simultaneously is shown in [8]. Here, significant landmarks are selected on the basis of a high-precision GPS and a high-precision map of the surroundings, from which the

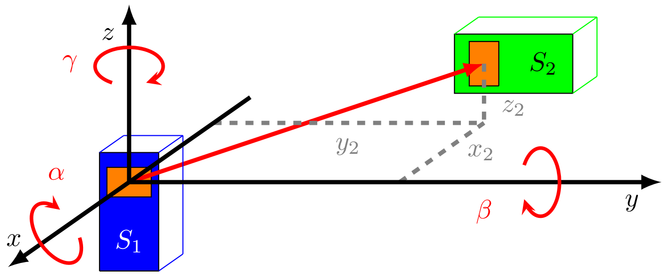

Fig. 1. Sketch of a radar sensor network consisting of two rotated and translated sensors in the reference coordinate system of the first sensor.

pose (position and orientation) is estimated. However, only the position in the xy-plane and the orientation around the z-axis can be estimated.

Using the algorithm presented in this paper, it is possible to determine the 3D orientation and the 3D position of all N radar sensors within a radar sensor network ($N{>}2$) in relation to each other. For this, only an overlapping field of view (FoV) of all N sensors and a moving point target, e.g. a corner reflector, are required, whose Ground-Truth trajectory and position do not need to be known. Moreover, no additional positioning system is needed and no prior knowledge is required.

For this purpose, the sensor set-up and the basics of the applied radar processing are described in Section II. Subsequently, Section III describes the algorithms for three-dimensional orientation and position estimation, which are subsequently evaluated in Section IV based on measurements with a precise robot-based ground truth.

II. Signal Processing

Precise radial velocities $v^{\mathrm{r,s}}_{n,m}$, azimuth incidence angles $\phi^{\mathrm{s}}_{n,m}$, elevation incidence angles $\theta^{\mathrm{s}}_{n,m}$, and distances $r^{\mathrm{s}}_{n,m}$ of M_n detected targets ($m{\le}M_n$, $n{\le}N$) can be determined with the help of N chirp-sequence radar sensors. For this purpose raw data of N externally triggered chirp-sequence radar sensors is stored, independently processed and transformed into the frequency domain using a fast Fourier transform (FFT). The relevant target information is extracted using a constant false alarm rate (CFAR), subsequent peak detection, and angle of arrival (AoA) estimation.

III. Pose Estimation Algorithm

An exemplary scenario of $N{=}2$ radar sensors is shown in Fig. 1 to illustrate the utilized coordinate system. Here, S_2

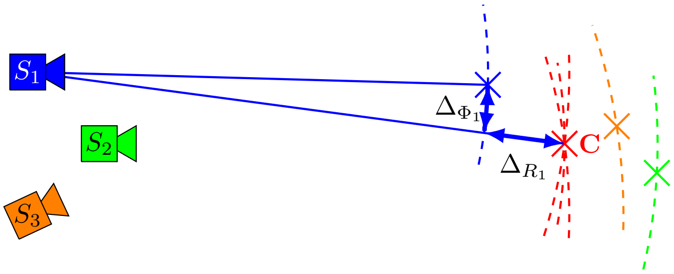

Fig. 2. Sketch of a radar sensor network consisting of three sensors and the associated detections and corresponding deviations from the most probable target position, which is shown in red.

is translated in all three dimensions and rotated around the x-axis, while S_1 always represents the origin of the utilized coordinate system.
The pose (position and orientation) estimate of the second sensor (n=2) in relation to the first sensor (n=1) has to be performed. In this case $\mathbf{T}_n$ denotes the translation and $\mathbf{R}_n$ the rotation of the n-th sensor in relation to the first sensor with

$$\mathbf{T}_n = \begin{bmatrix} x_n \\ y_n \\ z_n \end{bmatrix}, \mathbf{R}_n = \begin{bmatrix} \alpha_n \\ \beta_n \\ \gamma_n \end{bmatrix}, \tag{1}$$

where α describes the rotation around the x-axis, β the rotation around the y-axis, and γ the rotation around the z-axis. The proposed algorithm minimizes an error function g to estimate both the translation $\mathbf{T}_n$ and the rotation $\mathbf{R}_n$ for all N sensors. In order to avoid time-consuming approaches to match the different target lists of all sensors, only a moving point target or corner reflector is used, such that (M=1) holds. This can be achieved either by tracking the corner reflector, or in the case of a large corner reflector by a maximum search, as it is done in this work. All other detected targets are irrelevant and are neglected in the following.
Therefore, in the following, equations for the position estimation of a point target based on distributed radar sensors with overlapping FoV and known poses are derived first, as these can then be applied in an inverted way to precisely estimate the pose of the radar sensors.

A. Target Localization Based on Distributed Radar Sensors

Given known three-dimensional sensor positions and sensor orientations of N radar sensors, the most likely global target position $\mathbf{C}_f$ for a given frame f of a point target can be determined using a numerical minimization of squared error terms in spherical coordinates:

$$\mathbf{C}_f = \underset{x,y,z}{\arg\min} \underbrace{\left(\sum_{n=1}^{N} \left(\frac{\Delta R_n}{\sigma_\mathrm{r}}\right)^2 + \left(\frac{\Delta \Phi_n}{\sigma_\Phi}\right)^2 + \left(\frac{\Delta \Theta_n}{\sigma_\Theta}\right)^2 \right)}_{g} \tag{2}$$

The most likely target position $\mathbf{C}_f$ is exemplarily shown as a red cross and multi-sensor constellation in Fig. 2. For reasons of clarity, only in 2D, in the xy-plane.

The distance error ΔR_n, the azimuth error $\Delta \Phi_n$ and the elevation error $\Delta \Theta_n$ with respect to the resulting optimal target point $\mathbf{C}_f = [x, y, z]$ to be searched for, are minimized for all N sensors in their own local coordinate systems. These distance errors and angular errors are shown in Fig. 2 as blue arrows, respectively. σ_r, σ_Φ and σ_Θ represent normalization factors depending on the quality of the radar system and can be calculated according to [9], [10] as

$$\sigma_\mathrm{r} = \sqrt{\frac{3c_0^2}{(2\pi)^2 \,(\mathrm{SNR})\, N_\mathrm{sa} B^2}} \tag{3}$$

$$\sigma_\Phi = \frac{\Delta \Phi_\mathrm{3dB}}{1.6\sqrt{2\,(\mathrm{SNR})}} \tag{4}$$

$$\sigma_\Theta = \frac{\Delta \Theta_\mathrm{3dB}}{1.6\sqrt{2\,(\mathrm{SNR})}}, \tag{5}$$

where B describes the bandwidth, N_sa the number of samples per ramp, and Φ_3dB the 3dB angular separation capability. For the calculation of the sensor-wise distance errors ΔR_n, the azimuth errors $\Delta \Phi_n$, as well as the elevation errors $\Delta \Theta_n$ between all sensors and the optimal point $\mathbf{C}_f$. $\mathbf{C}_f$ is first transformed with the translation $\mathbf{T}_n$ and the rotation matrix $\mathbf{A}_n$ into the local coordinate system $\mathbf{C}_n^\mathrm{s}$ of the sensor n:

$$\begin{bmatrix} C_{\mathrm{x},n}^\mathrm{s} \\ C_{\mathrm{y},n}^\mathrm{s} \\ C_{\mathrm{z},n}^\mathrm{s} \end{bmatrix} = \mathbf{A}_n \left(\begin{bmatrix} C_\mathrm{x} \\ C_\mathrm{y} \\ C_\mathrm{z} \end{bmatrix} - \begin{bmatrix} x_n \\ y_n \\ z_n \end{bmatrix} \right). \tag{6}$$

Here $\mathbf{A}$ denotes the rotation matrix, which is composed as follows:

$$\mathbf{A}_n = \mathbf{A}_\mathrm{z}(\gamma_n)\, \mathbf{A}_\mathrm{y}(\beta_n)\, \mathbf{A}_\mathrm{x}(\alpha_n) \tag{7}$$

$$\mathbf{A}_\mathrm{x}(\alpha_n) = \begin{bmatrix} 1 & 0 & 0 \\ 0 & \cos(\alpha_n) & -\sin(\alpha_n) \\ 0 & \sin(\alpha_n) & \cos(\alpha_n) \end{bmatrix} \tag{8}$$

$$\mathbf{A}_\mathrm{y}(\beta_n) = \begin{bmatrix} \cos(\beta_n) & 0 & \sin(\beta_n) \\ 0 & 1 & 0 \\ -\sin(\beta_n) & 0 & \cos(\beta_n) \end{bmatrix} \tag{9}$$

$$\mathbf{A}_\mathrm{z}(\gamma_n) = \begin{bmatrix} \cos(\gamma_n) & -\sin(\gamma_n) & 0 \\ \sin(\gamma_n) & \cos(\gamma_n) & 0 \\ 0 & 0 & 1 \end{bmatrix} \tag{10}$$

A subsequent conversion into spherical coordinates allows the calculation of the quadratic error terms in the coordinate system which also corresponds to the measurable properties of a radar sensor. Subsequently, the most probable target position in local spherical coordinates in relation to the n-th radar sensor $\mathbf{C}_n^\mathrm{s}$ can be compared with the detected target position of the n-th radar sensor, which corresponds to the estimate from Section II. The conversion into spherical coordinates is done with

$$\begin{bmatrix} r_n^\mathrm{s,c} \\ \phi_n^\mathrm{s,c} \\ \theta_n^\mathrm{s,c} \end{bmatrix} = \begin{bmatrix} \sqrt{{C_{\mathrm{x},n}^\mathrm{s}}^2 + {C_{\mathrm{y},n}^\mathrm{s}}^2 + {C_{\mathrm{z},n}^\mathrm{s}}^2} \\ \mathrm{atan2}\left(C_{\mathrm{y},n}^\mathrm{s}, C_{\mathrm{x},n}^\mathrm{s}\right) \\ \mathrm{atan2}\left(C_{\mathrm{z},n}^\mathrm{s}, \sqrt{{C_{\mathrm{x},n}^\mathrm{s}}^2 + {C_{\mathrm{y},n}^\mathrm{s}}^2}\right) \end{bmatrix} \tag{11}$$

The distance and angular errors can subsequently be calculated as

$$\begin{bmatrix} \Delta R_n \\ \Delta \Phi_n \\ \Delta \Theta_n \end{bmatrix} = \begin{bmatrix} r_n^{\mathrm{s,c}} \\ \phi_n^{\mathrm{s,c}} \\ \theta_n^{\mathrm{s,c}} \end{bmatrix} - \begin{bmatrix} r_n^{\mathrm{s}} \\ \phi_n^{\mathrm{s}} \\ \theta_n^{\mathrm{s}} \end{bmatrix} . \tag{12}$$

These are shown in blue in Fig. 2 for a two-dimensional representation.

B. *Sensor Orientation Estimation*

The localization method presented above enables a precise estimation of a point target position based on distributed radar sensors with common FoV, which are all detecting the identical single target. For this purpose, a target position is determined which has the smallest square error in all three measurement dimensions to the target positions detected by the radar sensors. Based on this localization algorithm, an orientation estimation of the radar sensors can be performed. The sensor orientation for known sensor positions are added to the minimization problem in (2), such that both the target positions $\mathbf{C}_f$ as well as the sensor orientations $\mathbf{R}_n$ are optimized to produce a minimum error:

$$\mathbf{R}_{n\leq N} = \underset{\mathbf{R}_{n\leq N}}{\arg\min} \left(\min_{x,y,z} (g) \right) . \tag{13}$$

C. *Sensor Pose Estimation*

Since the orientation of the sensors does not change, (13) can be extended to evaluate not only a single frame f but F frames. Due to ambiguity regarding positioning and orientation, (13) can be extended to also include the positioning degrees of freedom as soon as at least $F{=}2$ frames are evaluated in order to determine the pose of the N radar sensors:

$$\left[\mathbf{T}_{n\leq N}, \mathbf{R}_{n\leq N}\right] = \underset{\mathbf{T}_{n\leq N},\mathbf{R}_{n\leq N}}{\arg\min} \left(\sum_{f=1}^{F} \min_{x,y,z} (g) \right) \tag{14}$$

With the help of minimization of the function g, the most probable target position $\mathbf{C}_f$ is determined for a given pose estimate and specific frame. The pose that provides the smallest square deviation between the detected target and the most probable target for all frames is the most probable one.

IV. Measurement Setup

The measurement setup for the verification of the algorithm consists of an incoherent radar network with $N{=}4$ chirp-sequence radar sensors and is shown in Fig. 3, for the reference position Fig. 3a and an arbitrary translation and rotation of the fourth sensor in Fig. 3b.

Three of the four sensors are positioned statically on the table while sensor S_4 is attached to a Kuka KRC4 robot. This allows millimeter translations and millidegree rotations around the antenna centre of the radar sensor [11]. The ground truth position of all sensors is determined with a tachymeter [12] with an accuracy of less than $2\,\mathrm{mm}$. Since no ground truth orientation of the radar sensors exists except for S_4, the orientation accuracy of sensors S_1, S_2 and S_3 is determined

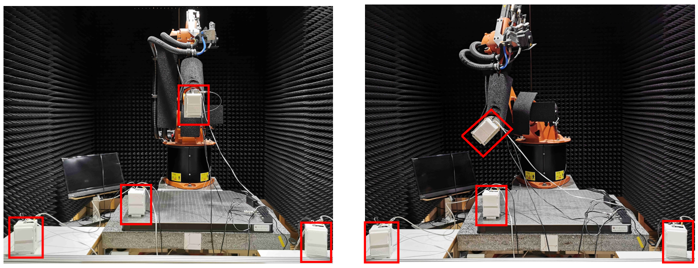

(a) (b)

Fig. 3. Measurement setup: (a) Reference position; (b) Translated and rotated radar sensor.

Table 1. Used Radar Parameters for Pose Estimation

Parameter	**Value**			
	S_1	S_2	S_3	S_4
Start frequency f_{start} (GHz)	77.22	77.25	77.28	77.34
Bandwidth B	3.06 GHz			
Ramp repetition time T_{r}	67 µs			
Sampling frequency f_{s} (IQ)	10 MHz			
Number of ramps (per Tx)	128			
Max. unambiguous velocity	$4.823\,\mathrm{m\,s^{-1}}$			
Number of transmitters	3			
Number of receivers	4			
Measurement rate	30 Hz			

using a differential calculation. Since these three sensors are stationary, the orientation must be identical regardless of the pose of S_4, which can be seen in Fig. 3a and Fig. 3b.

An external trigger is used to synchronize the sensors to ensure identical measurement times and to avoid interference between the sensors using different carrier frequencies. The radar parameters are shown in Tab. 1.

V. Measurement Results

In the following, the accuracy and robustness of the algorithm is evaluated with respect to different numbers of sensors and frames. The derived pose estimation method (14) is used to determine the position in all three dimensions as well as the orientation in 3D space of all $N{=}4$ sensors for different sensor orientations ($\alpha, \beta, \gamma \in [0°; 30°]$) of the fourth sensor, which is attached to the robot. For this purpose, a total of $F{=}10000$ frames per sensor and per orientation were recorded, which are then divided into 100 random sub-measurements of 1000 frames each to allow for 100 Monte Carlo iterations.

A. *Accuracy Analysis*

The average position errors and rotation errors of all sensors are visualized in Fig. 4.

The solid lines represent the average position error of all $N{=}4$ sensors, whereas the dashed lines represent the average differential rotation error of all $N{=}4$ sensors. The red lines represent the error of all sensors for a γ rotation of sensor S_4, whereas an $\alpha\beta\gamma$ rotation was applied to sensor S_4 for the resulting error in blue color. However, the estimation according to (14) is always performed for all six degrees of freedom without prior information.

Basically, it can be seen that the position of all four radar sensors can be determined with an accuracy up to $4\,\mathrm{cm}$.

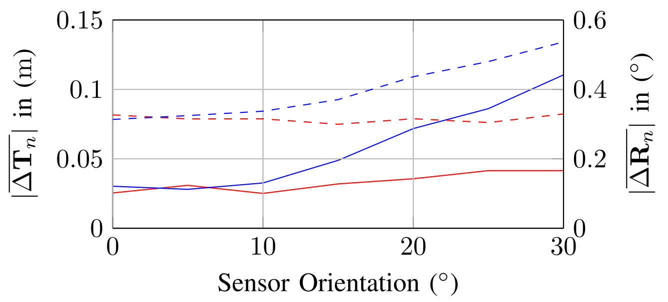

Fig. 4. Averaged translation error as solid lines and orientation error as dashed lines for N=4 radar sensors and F=1000 Frames for two different (red, blue) sensor rotations.

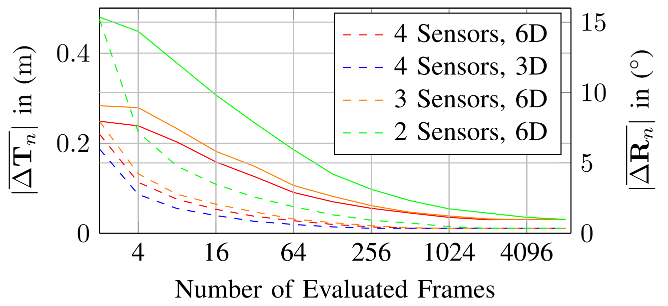

Fig. 5. Averaged translation error as solid lines and orientation error as dashed lines for different numbers of frames, sensor configurations, and dimensions: 6D - position and orientation, 3D - orientation.

Moreover the orientation can be estimated with an accuracy of up to $0.35°$ around all three axes.

However, for orientation angles larger than $10°$, the estimation of the sensors rotated around all three axes deteriorates significantly. It should be noted that this is due to hardware limitations of the sensors, which have a FoV of at least $60°$ in their local azimuth plane (xy-plane), their FoV in the local elevation plane (xz-plane) is restricted to $25°$. Since the trajectory of the corner reflector is mostly in the xy-plane and all sensors have to detect the corner reflector at identical times, the detected target points are located in a much smaller global area, which leads to a smaller angular difference and ultimately to a worse estimation. Furthermore, due to the reduced SNR, the detected target points have higher variances at elevation incidence angles close to or beyond $25°$, which also negatively affects the estimation.

As long as a large overlapping FoV of all sensors is given despite rotation, even a large α rotation of $45°$ as shown in Fig. 3b can be determined with an accuracy of $0.35°$. Here, the position accuracy is also similar to $3.8\,\mathrm{cm}$.

B. Robustness

According to (14), at least two sensors and two frames must be evaluated for the 6D pose estimation. The average accuracy for different frame numbers as well as different numbers of sensors is shown in Fig. 5.

It can be seen that as the number of evaluated frames increases, the accuracy of the orientation estimation and the position estimation improves significantly. Furthermore, the accuracy can also be improved by additional sensors. This is the consequence of a more precise target position determination $\mathbf{C}$ using (2), which in turn results in improved pose estimates based on (14).

If the position of the sensors is already known and only the orientation of the sensors has to be estimated, the estimation accuracy increases by $20\,\%$. This is shown by the red and blue lines respectively for N=4 sensors in Fig. 5.

VI. Conclusion

The presented algorithm allows both a relative position estimation and a relative orientation estimation of all radar sensors in a radar sensor network with overlapping FoVs. It was shown by measurements that the 3D position of all radar sensors can be determined with an average accuracy of $4\,\mathrm{cm}$. Moreover, the average accuracy for 3D orientation estimation was shown to be $0.35°$. Since the evaluation time of the algorithm for 1000 frames takes only seconds and only target lists and a moving corner reflector are required for the algorithm, precise pose information can be obtained quickly and with high precision making the algorithm well suited for experimental setups e.g. variable sensors mounted on a vehicle.

References

[1] C. Waldschmidt, J. Hasch, and W. Menzel, "Automotive Radar — From First Efforts to Future Systems," *IEEE J. Microw.*, vol. 1, pp. 135–148, 2021.

[2] M. Steiner, O. Hammouda, and C. Waldschmidt, "Ego-Motion Estimation using Distributed Single-Channel Radar Sensors," in *IEEE MTT-S Int. Conf. Microw. Intell. Mobil. (ICMIM)*, Apr. 2018, pp. 1–4.

[3] J. Pierre and M. Kaveh, "Experimental performance of calibration and direction-finding algorithms," in *[Proceedings] ICASSP 91: 1991 Int. Conf. on Acoust., Speech, and Signal Process.*, 1991, pp. 1365–1368 vol.2.

[4] C. Vasanelli, F. Roos, A. Durr, J. Schlichenmaier, P. Hugler, B. Meinecke, M. Steiner, and C. Waldschmidt, "Calibration and Direction-of-Arrival Estimation of Millimeter-Wave Radars: A Practical Introduction," *IEEE Antennas Propag. Mag.*, vol. 62, no. 6, pp. 34–45, 2020.

[5] A. Dürr, M. Linder, D. Schwarz, and C. Waldschmidt, "Highly Efficient Angular Array Calibration Based on the Modal Wave Expansion Technique," *IEEE Open J. Antennas Propag.*, vol. 2, pp. 938–948, 2021.

[6] D. Kellner, M. Barjenbruch, K. Dietmayer, J. Klappstein, and J. Dickmann, "Joint radar alignment and odometry calibration," in *2015 18th Int. Conf. on Inf. Fusion (Fusion)*, 2015, pp. 366–374.

[7] M. Z. Ikram and A. Ahmad, "Automated Radar Mount-Angle Calibration in Automotive Applications," in *2019 IEEE Radar Conf. (RadarConf)*, 2019, pp. 1–5.

[8] R. Izquierdo, I. Parra, D. Fernández-Llorca, and M. A. Sotelo, "Multi-Radar Self-Calibration Method using High-Definition Digital Maps for Autonomous Driving," in *2018 21st Int. Conf. on Intell. Transp. Syst. (ITSC)*, 2018, pp. 2197–2202.

[9] H. Griffiths, "Radar System Analysis and Modeling." *The Aeronautical Journal*, vol. 109, p. 591, 11 2005.

[10] S. Scherr, R. Afroz, S. Ayhan, S. Thomas, T. Jaeschke, S. Marahrens, A. Bhutani, M. Pauli, N. Pohl, and T. Zwick, "Influence of Radar Targets on the Accuracy of FMCW Radar Distance Measurements," *IEEE Trans. Microw. Theory Tech.*, vol. 65, no. 10, pp. 3640 – 3647, 2017.

[11] L. Boehm, F. Boegelsack, M. Hitzler, and C. Waldschmidt, "The Challenges of Measuring Integrated Antennas at Millimeter-Wave Frequencies [Measurements Corner]," *IEEE Antennas Propag. Mag.*, vol. 59, no. 4, pp. 84–92, 2017.

[12] *Trimble Universale Total Station SPS930*, 2018.